NONLINEAR LOCAL BENDING RESPONSE AND BULGING FACTORS FOR LONGITUDINAL AND CIRCUMFERENTIAL CRACKS IN PRESSURIZED CYLINDRICAL SHELLS

Richard D. Young,[*] Cheryl A. Rose,[*] and James H. Starnes, Jr.[†]
NASA Langley Research Center
Hampton, Virginia 23681-001

Abstract

Results of a geometrically nonlinear finite element parametric study to determine curvature correction factors or "bulging factors" that account for increased stresses due to curvature for longitudinal and circumferential cracks in unstiffened pressurized cylindrical shells are presented. Geometric parameters varied in the study include the shell radius, the shell wall thickness, and the crack length. The major results are presented in the form of contour plots of the bulging factor as a function of two nondimensional parameters: the shell curvature parameter, λ, which is a function of the shell geometry, Poisson's ratio, and the crack length; and a loading parameter, η, which is a function of the shell geometry, material properties, and the applied internal pressure. These plots identify the ranges of the shell curvature and loading parameters for which the effects of geometric nonlinearity are significant. Simple empirical expressions for the bulging factor are then derived from the numerical results and shown to predict accurately the nonlinear response of shells with longitudinal and circumferential cracks. The numerical results are also compared with analytical solutions based on linear shallow shell theory for thin shells, and with some other semi-empirical solutions from the literature, and limitations on the use of these other expressions are suggested.

Introduction

The fail-safe design philosophy applied to transport aircraft fuselage structure requires that these structures retain adequate structural integrity in the presence of discrete source damage or fatigue cracks. Two types of damage most frequently associated with the structural integrity of fuselage structures are longitudinal cracks subjected to the hoop stresses resulting from the internal pressure loads, and circumferential cracks subjected to stresses resulting from the vertical bending and shearing of the fuselage induced by normal flight loads. The analysis of these fuselage cracks is complex due to the geometric coupling of the bending and stretching deformations that is characteristic of any shell, the geometrically nonlinear stiffening effect of membrane tensile stresses that are aligned with the crack faces, and the interaction of the crack with the surrounding structure (frames, stiffeners, and tear straps). To make the residual strength analyses of fuselage structure

[*]Aerospace Engineer, Mechanics and Durability Branch.
[†]Chief Engineer, Structures and Materials Competency

tractable in the design phase, current residual strength analyses and damage tolerant design practice rely primarily on geometrically linear analyses and fracture analyses based on linear elastic fracture mechanics. Linear elastic fracture mechanics suggests that the strength of the stress singularity at the crack tip, or the crack-tip stress intensity factor, is an indicator of the likelihood of fracture. The conventional engineering approach used in design practice is to predict the crack-tip stress intensity factors for a crack in a fuselage shell by applying a so-called "bulging factor," in combination with additional design factors that account for stiffener elements, to the stress intensity factor for a flat plate subjected to similar loading conditions. The bulging factor accounts for the fundamental difference in behavior of a crack in a curved shell compared to the behavior of a crack in a plate. In a cracked shell, the local region around the crack deforms out-of-plane as a result of the curvature induced coupling between the membrane and bending actions, and the internal pressure, where in a plate, the crack deforms in plane. These out-of-plane displacements in the neighborhood of a crack in a shell increase the crack opening and crack-tip stress intensity compared to those of a cracked plate with the same crack geometry. The bulging factor amplifies the flat-sheet stress intensity factor and is defined as the ratio of the stress intensity factor in a cracked shell to the stress intensity factor in a cracked plate.

Many studies have been conducted to characterize bulging cracks, and both analytical[1-8] and empirical formulas[9-14] for the bulging factor have been developed. Analytical expressions for the bulging factor in shells were first developed by Folias using a formulation based on linear shallow-shell theory.[1-4] Folias' expressions depend on the shell curvature parameter, λ, where, for an isotropic shell, λ is defined as:

Equation 1:

$$\lambda = \frac{a}{\sqrt{Rt}} \sqrt[4]{12(1-\nu^2)}$$

and:

ν = *Poisson's ratio*

a = *half crack length*

R = *radius of the shell*

t = *thickness of the shell*

Folias' original solutions are only valid for very small values of λ. The range of application of his solutions was later extended[5-8] to larger values of λ ($\lambda = 8$ for a longitudinal crack, $\lambda = 10$ for a circumferential crack), by solving numerically the integral equations associated with the problem.

For a longitudinal crack in a shell subjected to internal pressure loads, and a circumferential crack in a shell subjected to axial tension loads, the analytical bulging factors tend to overestimate the physical bulging effect, unless the cracks are very short, or the applied load is very small, so that geometric nonlinear effects are not significant. The error introduced by the linearization of the shell equations has been explained by Riks, et al.,[15] and is a result of the tensile membrane stresses that develop along the crack edges as the crack bulges. These tensile stresses increase the resistance to additional crack bulging and crack opening. This nonlinear coupling between the bulging

deformations and the membrane tensile stresses is not predicted by a linear analysis. Recently, some empirical formulas for determining bulging factors in shells with longitudinal cracks, which attempt to account for the nonlinear character of the bulging response, have been developed. These empirical formulas were developed for specific materials, geometries and loading conditions, and thus, the validity of the formulas is limited to certain applications. These formulas may lead to unsafe designs if their predictions are non-conservative, or conversely, to excessive structural weight if they are overly conservative.

A more general investigation of the effects of geometric nonlinearities on the response of cylindrical shells with longitudinal cracks was conducted by Budiman and Lagace.[16,17] Using the Donnell-Mushatari-Vlasov nonlinear shallow shell theory,[18] Budiman and Lagace postulated that the nonlinear response is dependent on two nondimensional parameters: the shell curvature parameter, λ, which appears in the linear theory, and is defined in Eq. (1); and a loading parameter, η, which depends on the applied internal pressure, material properties, and shell geometry. From the nondimensional form of the governing equations, Budiman and Lagace[16] defined η as

Equation 2:

$$\eta_{Budiman} = \left(\frac{pR}{t}\right)\frac{1}{E}\frac{1}{\left(\frac{t}{R}\right)}$$

where:

$$E = \textit{Young's modulus}$$

$$p = \textit{internal pressure}$$

and the remaining variables are as defined in Eq. (1). Budiman and Lagace stated that η is a measure of the "driving force" of the nonlinearity. Budiman and Lagace assessed the applicability of these parameters to the nonlinear response of cylindrical shells with longitudinal cracks by conducting nonlinear analyses of different cylindrical configurations using the STAGS finite element code.[19] The results of the analysis showed that the two parameters are able to characterize the response of cylindrical shells with longitudinal cracks. Budiman[17] also suggested, after obtaining the same two parameters from the nondimensional form of Sanders' nonlinear shell equations, that λ and η can be used to characterize the response of cylindrical shells when the crack is oriented in the circumferential direction. Sanders' nonlinear shell equations,[18] which are valid for deep shells, are required for a cylindrical shell with a circumferential crack, because the crack length influences the shallowness assumption. Budiman, however, did not determine if these parameters adequately characterize the response of cylindrical shells with circumferential cracks.

The present paper has several objectives. The first objective is to present the results of a comprehensive geometrically nonlinear numerical parametric study of the response of aluminum shells with centrally located longitudinal and circumferential cracks subjected to internal pressure and the associated bulkhead loads. The numerical analysis is conducted using the STAGS (STructural Analysis of General Shells) nonlinear finite element code.[19] Geometric parameters varied in the parametric study include the shell radius, the shell wall thickness, the crack length, and the crack orientation. The second objective is to assess the dependence of the nonlinear response of shells

with circumferential cracks on the two parameters λ and η. The third objective is to develop simple expressions for the bulging factors for longitudinal and circumferential cracks in cylindrical shells, that can be easily used in a design environment. The final objective is to summarize and assess some of the approximate analytical and empirical expressions that have been developed for predicting bulging factors for use in crack growth and residual strength analyses of fuselage shells. The accuracy and range of applicability of the approximate expressions are assessed through comparisons with the present geometrically nonlinear analysis results. Results are presented in contour plots that show the bulging factor as a function of the shell curvature parameter, λ, and the loading parameter, η.

Strain-Energy Release Rate and Bulging Factor

Linear elasticity theory predicts a stress singularity at the tips of cracks, and in the case of a flat plate, the stress singularity has the character of the inverse square root of the distance from the crack tip. The strength of the crack-tip stress field singularity is represented by the stress intensity factor, K, which has been suggested as being significant in determining the likelihood of crack extension. For a flat plate, or in cases when the linear shell equations apply, the crack-tip stress field and the stress intensity factor are proportional to the loads, and the stress intensity factors can be related to the strain-energy release rate.[20] For a flat plate with a central crack subjected to uniaxial tension perpendicular to the crack direction, the stress intensity factor, K_p, is defined as:

Equation 3:

$$K_p = \sigma\sqrt{\pi a}\, f(W)$$

where σ is the in-plane remote stress acting perpendicular to the crack line, and $f(W)$ is a function to account for finite width effects. For the traditional Mode I type loading condition, where the applied tensile load is perpendicular to the crack line, the relationship between the stress intensity factor and the strain-energy release rate, G, has the form:

Equation 4:

$$G = \frac{K_p^{\,2}}{E}$$

where E is Young's modulus. When geometrically nonlinear effects are present, the stress field, and hence the stress intensity factor, are not linear functions of the applied load, and the stress intensity factor cannot be defined as in Eq. (3). To address this problem, an engineering approach is employed and the nonlinear stress intensity factor for the shell, K_s, is defined on the basis of Eq. (4).[21] For the present study, the stress intensity factor K_s is calculated from:

Equation 5:

$$K_s = \sqrt{EG}$$

For the symmetric loading conditions considered in the present paper, K_s defined by Eq. (5) is the total stress intensity factor, and is a combination of the symmetric membrane and bending stress intensity factors, K_I and k_1, respectively.[22] In the present paper, only the total stress intensity factor K_s is considered. The stress intensity factor K_s is related through a bulging factor to the stress intensity factor for the reference problem of a flat plate with a central crack subjected to uniaxial tension perpendicular to the crack direction. The bulging factor, β, is defined as the ratio of the stress intensity factor K_s in a shell with a crack, to the stress intensity factor K_p in a flat plate of the same material, thickness, crack length, and in-plane remote stress, σ, acting perpendicular to the crack line:

Equation 6:

$$\beta = \frac{K_s}{K_p}$$

In the present study, the bulging factor for a cylindrical shell with a longitudinal crack or a circumferential crack is denoted as β^L and β^C, respectively.

Shell Geometry and Analysis Procedure

Shell Model

The geometry of a typical shell analyzed in the present study is defined in Fig. 1. The shell shown in Fig. 1 is a segment of an infinitely long cylindrical shell, with an infinite number of equal length longitudinal or circumferential cracks evenly distributed along the length of the shell to maintain the symmetry of the models. The shell is made of 2024-T3 aluminum alloy and has a

Figure 1. Shell Geometry.

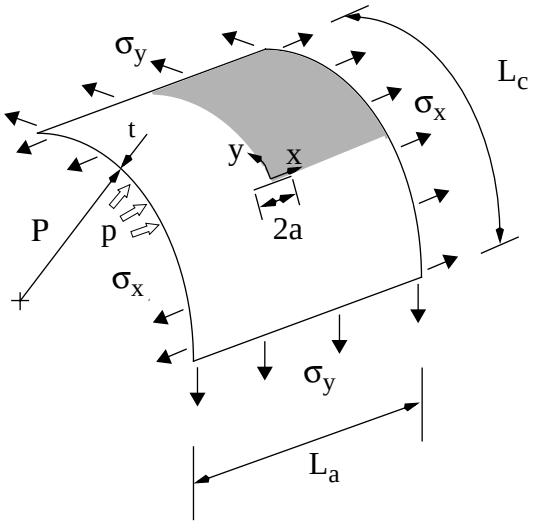

radius, R, an axial length, L_a, a circumferential length, L_c, a wall thickness, t, and a crack length, $2a$. The crack is centrally located and is oriented longitudinally (parallel to the x-axis) or circumferentially (parallel to the y-axis). The Young's modulus, E, for the aluminum alloy is equal to 10.35 msi and Poisson's ratio, ν, is equal to 0.3.

Typical finite element models used to simulate the response of the cracked shells are shown in Fig. 2, for shells with two different crack orientations. Quarter symmetry was assumed, so only the shaded portion of the shell segment shown in Fig. 1 was modeled. To simplify model generation for the wide range of parameters considered, the model dimensions in the x and y directions, and the element dimensions were scaled by the crack length. This approach was used to reduce the effort required to model shells with different crack lengths, while maintaining reasonable consistency in the solution resolution in going from a mesh for a short crack to a mesh for a long crack. The dimensions of the models in the x and y directions were set equal to $24a$ and $6a$, respectively. These dimensions were chosen to reduce finite width and finite length effects to an acceptable level; that is, changing the edge conditions resulted in less than a 5% change in the computed stress intensity factor. The longer dimension in the longitudinal direction was required to minimize edge effects for the cylindrical shell with a circumferential crack.

The shells were modeled using STAGS standard 410 quadrilateral shell elements, and 510 and 710 mesh-transition elements, where needed. The elements are flat facet-type elements and are based on Kirchoff-Love shell theory and the nonlinear Lagrangian strain tensor.[19] Each of the shell element nodes has six degrees of freedom, including three translational degrees of freedom,

Figure 2. Typical finite element models.

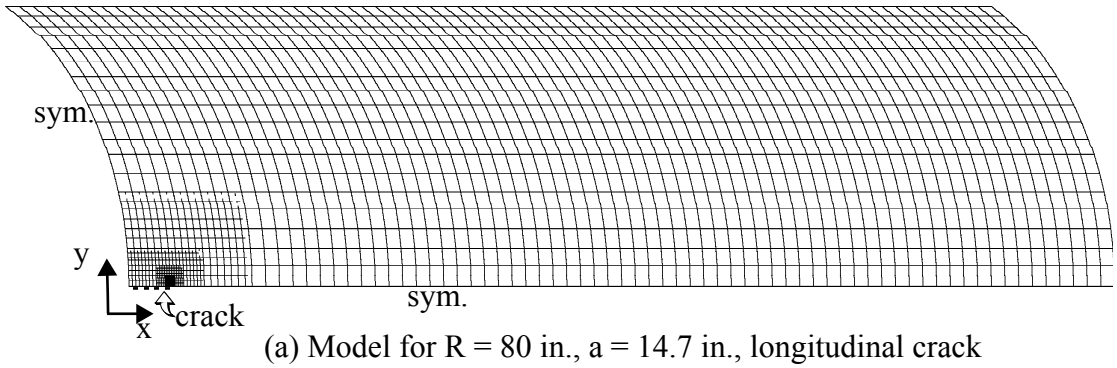

(a) Model for R = 80 in., a = 14.7 in., longitudinal crack

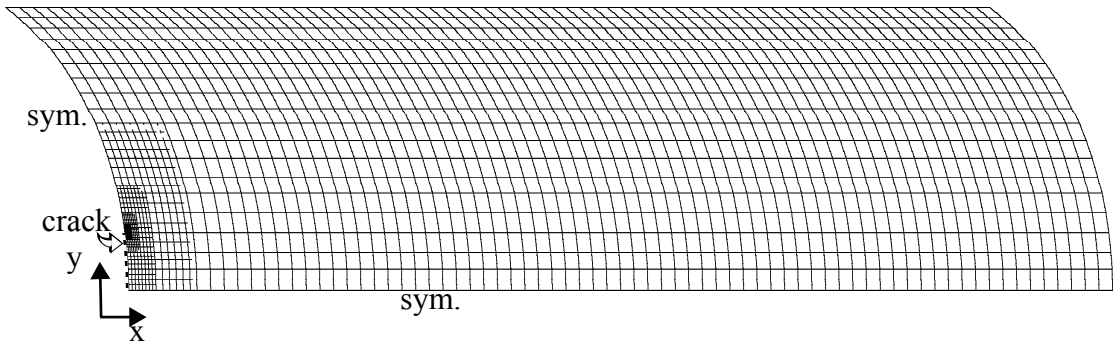

(b) Model for R = 80 in., a = 14.7 in., circumferential crack

u, v, and w, and three rotational degrees of freedom, ru, rv, and rw about the axes x, y, and z, respectively (see Fig. 1). Symmetry boundary conditions were prescribed on the left ($x = 0$) and bottom ($y = 0$) edges of the model. Periodic boundary conditions were prescribed to approximate the physical boundary conditions on the top ($y = 6a/R$) and right edges ($x = 24a$) of the model. The right edge of the model was also constrained to remain cylindrical throughout the loading process. Specifically, on the top edge of the model, the circumferential degree of freedom, v, and the rotational degrees of freedom, ru, and rw, were set equal to zero; and on the right edge of the model, the axial and radial degrees of freedom, u, and w, respectively, were constrained to be uniform, and the rotational degrees of freedom, rv, and rw, were set equal to zero. A symmetric crack with only one side of the crack modeled was defined along the bottom edge (longitudinal crack) or left edge (circumferential crack) of the model. The crack has a half crack length equal to a and starts in the lower left corner of the model and extends to the right (longitudinal crack), or up (circumferential crack), as shown in Fig. 2. A fine mesh was required to represent the stress and deformation gradients near the crack tip. To eliminate the dependence of the results on mesh resolution, several analyses were conducted, with increasing mesh refinement in the crack-tip region, until further refinement produced less than 1% change in the total stress intensity factor, K_s. The analyses converged using elements near the crack tip with edge lengths equal to $0.01a$. Predictions of the flat-plate stress intensity factor using the converged mesh were within 1% of the predictions obtained using Eq. (3), with Irwin's finite width adjustment.[20] An internal pressure load was applied to the shell. Internal pressure was simulated by applying a uniform lateral pressure to the shell wall and an axial tensile force to account for bulkhead pressure loads to the right edge of the shell, $\sigma_x = (\sigma_y/2)$, with multi-point constraints to enforce a uniform edge displacement.

Nonlinear Analysis Procedure

The shell responses were predicted numerically using the STAGS (STructural Analysis of General Shells) nonlinear shell analysis code.[19] STAGS is a finite element code for general-purpose analysis of shells of arbitrary shape and complexity. STAGS analysis capabilities include stress, stability, vibration and transient response analyses, with both material and geometric nonlinearities represented. The code uses both the modified and full Newton methods for its nonlinear solution algorithms, and accounts for large rotations in a shell by using a co-rotational algorithm at the element level. The Riks pseudo arc-length path following method[23,24] is used to continue a solution past limit points in a nonlinear response. With this method, the incrementally applied loading parameter is replaced by an arc-length along the solution path which is then used as an independent loading parameter. The arc-length increments are automatically adjusted by the program as a function of the solution behavior. The strain-energy release rate is calculated in STAGS, from a nonlinear equilibrium state, using the modified crack closure integral technique.[25]

Results and Discussion

The geometrically nonlinear analysis results for unstiffened cylindrical shells with a longitudinal or circumferential crack are presented in this section. This section is separated into four parts. The first three parts each correspond to a different phase in the nonlinear analysis approach that was used to assess the applicability of the nondimensional parameters λ and η for characterizing

the nonlinear response of a shell with a crack, and to study the effect of these parameters on the nonlinear shell response. In the first part, the accuracy of the analysis model and the analysis procedure is assessed by comparing the STAGS linear predictions for the bulging factor, with solutions in the literature that are based on linear shallow shell theory. The linear analyses were performed for 30 shells with a radius equal to 80 in., a shell wall thickness equal to 0.040 in., and half-crack lengths ranging from 0.49 in. to 14.76 in. In the second part, results of the analyses conducted for the specific shell configurations shown subsequently in Table 1 are presented to confirm the applicability of the nondimensional parameters λ and η for characterizing the nonlinear response of shells with longitudinal and circumferential cracks. The shell configurations shown in Table 1 represent a variation of the shell curvature parameter of $2.875 \le \lambda \le 11.50$. The third part presents results of a series of nonlinear analyses that were conducted to determine the bulging factors for a large range of the nondimensional parameters. Simple empirical expressions for the bulging factor are then derived from the numerical results and shown to predict accurately the nonlinear response of shells with longitudinal and circumferential cracks. In all of the analyses, the loading condition for the shell consisted of an applied internal pressure, *p*, which generates a hoop stress reaction, σ_y, and an axial stress, $\sigma_x = \sigma_y/2$, which is a bulkhead pressure load, giving a biaxial load ratio $\chi = \sigma_x/\sigma_y = 0.5$. For pressurized shells, different values of the biaxial load ratio can exist if an additional mechanical load is applied to the ends of the shell. Previous studies have shown that the bulging factor for shells with longitudinal cracks is sensitive to the biaxial load ratio,[11,26] but the present study was limited to the 'pressure only' case. Internal pressure was varied such that $0 \le \eta \le 3.0$, where in the present study the loading parameter, η, is defined as:

Equation 7:

$$\eta = \sqrt{\frac{\sigma}{E}\frac{R}{t}}\left(\sqrt[4]{12(1-\nu^2)}\right)$$

where σ is the in-plane remote stress acting perpendicular to the crack line:

$$\sigma = p\frac{R}{t}$$, for a shell with a longitudinal crack, and

$$\sigma = p\frac{R}{2t}$$, for a shell with a circumferential crack.

Finally, in the last section, the bulging factor results from the present nonlinear analysis are compared with bulging factor results from empirical expressions that approximately account for the geometric nonlinearity.[11-14] All computations were performed using $E = 10.35$ msi and $\nu = 0.3$.

Linear Bulging Factors for Shells with Longitudinal and Circumferential Cracks

In a linear analysis, the bulging factor depends only on the shell curvature parameter, λ. The linear bulging factors as a function of λ, computed using a linear STAGS analysis, are compared in Fig. 3 with bulging factors computed from numerical solutions that are based on linear shallow shell theory. The linear bulging factors for a shell with a longitudinal crack, β_{lin}^{L}, and for a shell with a circumferential crack, β_{lin}^{C}, are shown in Figs. 3a and 3b, respectively. The numerical

solutions from the literature are available for values of λ less than 8 for the case of a longitudinal crack,[6] and for values of λ less than 10 for the case of a circumferential crack.[7] The predictions shown in Fig. 3 were obtained using a configuration with a radius, R = 80 in., thickness, t = 0.040 in., and with the half-crack length, a, varied to provide the range of λ values shown. The agreement between the geometrically linear finite element predictions, shown by the symbols, and the numerical solutions presented in Refs. 6 and 7, shown by the solid lines, is excellent, indicating that the mesh refinement near the crack tip, and that the shell length chosen for the models, are adequate.

Figure 3. Linear bulging factors versus λ, predicted using STAGS and the numerical solution of Erdogan and Kibler[6] (longitudinal crack), and Erdogan and Ratwani[7] (circumferential crack).

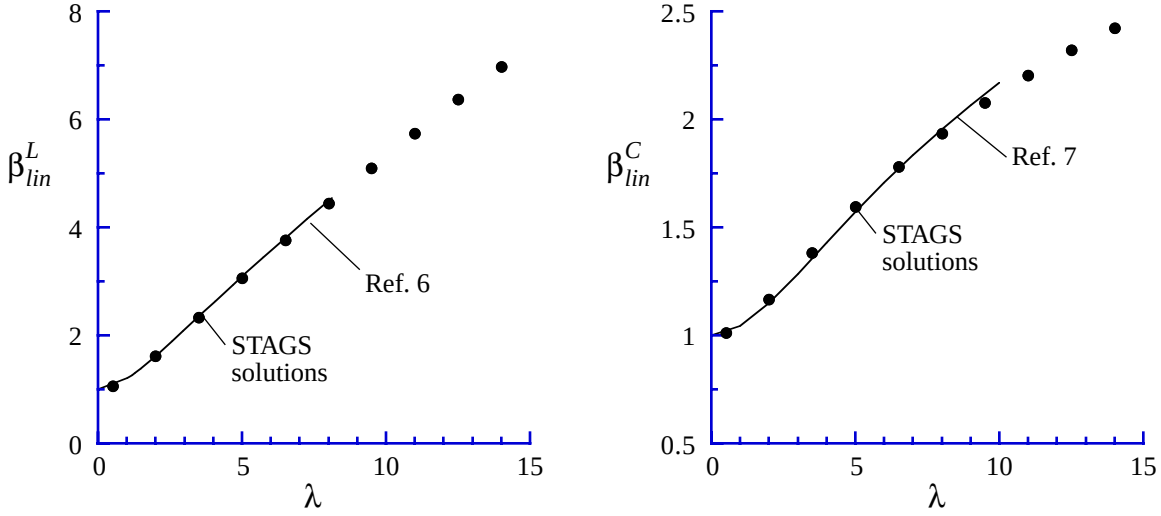

(a) Linear bulging factor for a longitudinal crack, β^L_{lin}.

(b) Linear bulging factor for a circumferential crack, β^C_{lin},.

Assessment of λ and η as Governing Parameters for the Nonlinear Response of Shells with Longitudinal and Circumferential Cracks

Following Budiman and Lagace,[16] the second step in the analysis was to confirm the applicability of the shell curvature parameter, λ, and the loading parameter, η, for characterizing the nonlinear response of cylindrical shells with both longitudinal and circumferential cracks. Cylindrical shell configurations considered in this phase of the analysis are provided in Table 1. As shown in Table 1, sixteen different cylindrical shell configurations with values of λ equal to 2.875, 5.75, 8.625, and 11.50 were considered. For each value of λ, nonlinear analyses were performed for two values of the shell radius, and shell wall thickness, with the half-crack length adjusted accordingly. The larger radius, R = 80 in., is representative of a narrow-body fuselage geometry, and the smaller radius, R = 20 in., is representative of relatively large laboratory scale specimen.

Budiman and Lagace confirmed that the nondimensional parameters λ and η, obtained from the governing equations, can be used to characterize the response of cylindrical shells with longitudinal cracks by showing that the nonlinear bulging factor response for a shell with a longitudinal

Table 1. Configurations considered to confirm the applicability of nondimensional parameters, λ and η.

		λ = 2.875	λ = 5.75	λ = 8.625	λ = 11.50
R=20 in.	t=0.02 in.	a = 1 in.	a = 2 in.	a = 3 in.	a = 4 in.
	t=0.08 in.	a = 2 in.	a = 4 in.	a = 6 in.	a = 8 in.
R=80 in.	t=0.02 in.	a = 2 in.	a = 4 in.	a = 6 in.	a = 8 in.
	t=0.08 in.	a = 4 in.	a = 8in.	a = 12 in.	a = 16 in.

crack, when plotted as a function of η for different cylindrical shell configurations, collapses to a single curve for a constant value of λ. Similar results were obtained in the present analysis and are presented in Fig. 4 for completeness. The nonlinear analysis results for the bulging factor of a shell with a longitudinal crack, β^L, of the configurations outlined in Table 1 are shown in Fig. 4 as a function of the loading parameter, η, for the four different values of λ. For each value of λ in Table 1, there are four cylindrical shell configurations. Therefore, each curve in Fig. 4, labeled with a constant value of λ, corresponds to the bulging factor predictions for four different configurations. The results in Fig. 4 show that the bulging factor response is a nonlinear function of the loading parameter, η, for all values of λ. For all values of λ, and small values of η (η<<1) the local shell response is predominantly a linear bending response, and the bulging factors from the nonlinear analysis depend only on λ, and are therefore independent of the loading parameter, η. The linear response is indicated by the flat regions of the curves in Fig. 4. For larger values of η, the response transitions from a linear bending dominated response to a nonlinear membrane dominated response, where the bulging factor is dependent on the loading parameter and decreases with increasing load. The reduction in the bulging factor with increase in the loading parameter is a result of the geometrically nonlinear coupling between the axial tensile stresses that develop along the crack edges and the crack bulging deformations. For configurations with large values of λ (longer crack lengths), the response is more nonlinear than for shells with small values of λ (shorter crack lengths), as indicated by the steeper slopes of the curves with larger values of λ. This trend is consistent with the results obtained by Budiman and Lagace.[16]

Budiman[17] also suggested that λ and η can be used to characterize the response of cylindrical shells when the crack is oriented in the circumferential direction. Budiman, however, did not conduct any analyses to determine if λ and η adequately characterize the nonlinear response of circumferentially cracked cylindrical shells. In the present study nonlinear analyses were conducted for the same shell configurations as for the longitudinal crack (Table 1), to assess the applicability of these parameters for circumferentially cracked cylindrical shells. Results of the nonlinear analyses are summarized in Figs. 5 and 6. The results of the nonlinear analyses for different shells with circumferential cracks having λ = 2.875 are shown in Fig. 5. The results in Fig. 5a show that the nonlinear bulging factor for a shell with a circumferential crack, β^C, is strongly dependent on the specific shell geometry and the longitudinal stress, σ_x. The linear solution for the bulging factor corresponds to the nonlinear bulging factor results for $\sigma_x = 0$. For all of the configurations shown, the magnitude of the bulging factor decreases as the applied stress increases. Furthermore, geometric nonlinear effects become important for very small values of the applied stress σ_x, as indicated by the immediate decline in the magnitude of the bulging factor for values of $\sigma_x > 0$ for all of the shell geometries studied.

Figure 4. Dependence of the bulging factor for a longitudinal crack, β^L, on the loading parameter, η, for several values of the shell curvature parameter, λ.

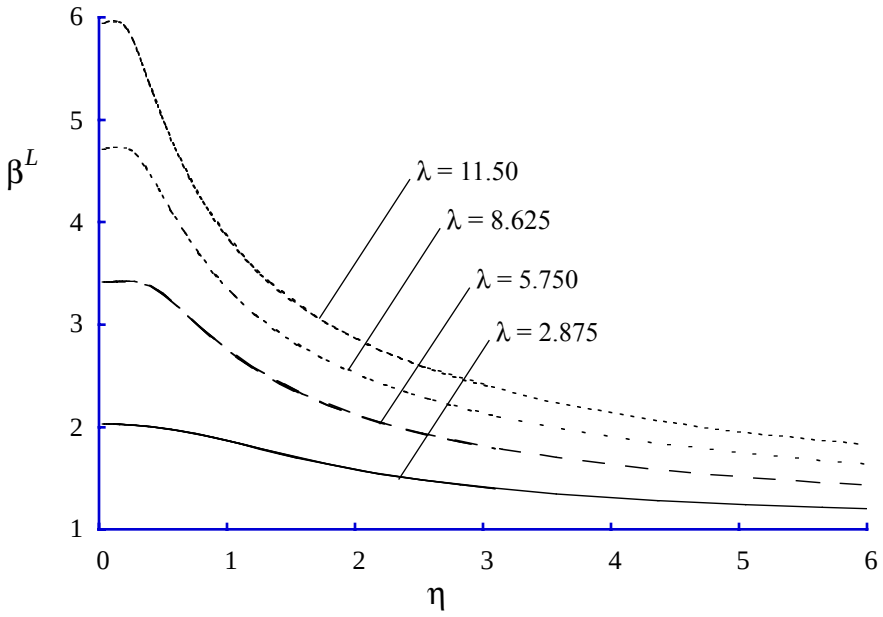

In Fig. 5b the nonlinear bulging factors are presented as a function of η for the four different cylinders that have $\lambda = 2.875$. The linear bulging factor results are obtained from the nonlinear results when $\eta = 0$. The results in Fig. 5b show that when the nonlinear bulging factors are presented as a function of η, the response for the different shells presented in Fig. 5a collapse to a single curve. Similar results are obtained for shells with different values of λ. As shown in Fig. 6, the bulging factors for circumferential cracks, β^C, for the 16 configurations in Table 1 collapse to four lines, or one line for each value of λ, when shown as a function of η. Therefore, the results of the analyses confirm the use of the parameters λ and η to characterize the nonlinear response of shells with circumferential cracks. Furthermore, for a given shell and crack length (given λ), geometric nonlinearities affect the bulging response, as indicated by the dependence of the bulging factor on the loading parameter. For a given shell, the longer the crack length (larger λ), the more nonlinear the response, as indicated by the steeper slopes of the curves with larger values of λ.

Bulging Factors for a Large Range of the Nondimensional Parameters

Having shown that the nonlinear shell response is characterized by λ and η, a series of nonlinear analyses were conducted to determine the bulging factors for a large range of the nondimensional parameters. These analyses were conducted using shell configurations with R = 80.0 in., t = 0.04 in., and half-crack lengths to provide values of $0.5 \le \lambda \le 15$ in increments of 0.5, and the internal pressure was varied such that $0 \le \eta \le 3.0$.

Longitudinal Crack

The bulging factors from STAGS analyses of cylindrical shells with longitudinal cracks, β^L, as a function of the shell curvature parameter, λ, and the loading parameter, η, are presented as a contour plot in Fig. 7. The solid lines in the figure are contour lines, or lines through points with

Figure 5. Dependence of the bulging factor for a circumferential crack, β^C, on the loading values, for configurations with $\lambda = 2.875$.

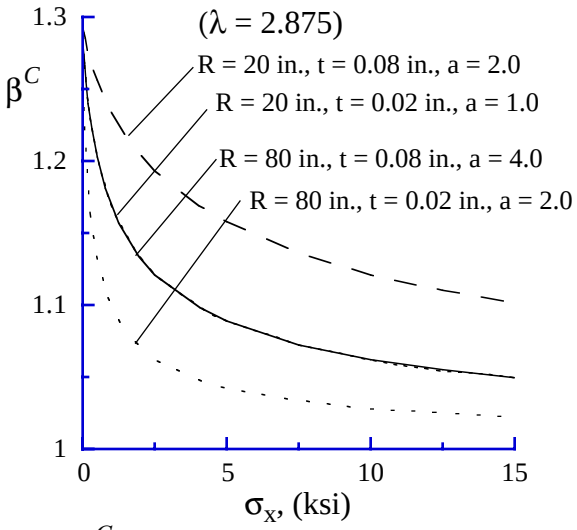

(a) β^C as a function of longitudinal stress

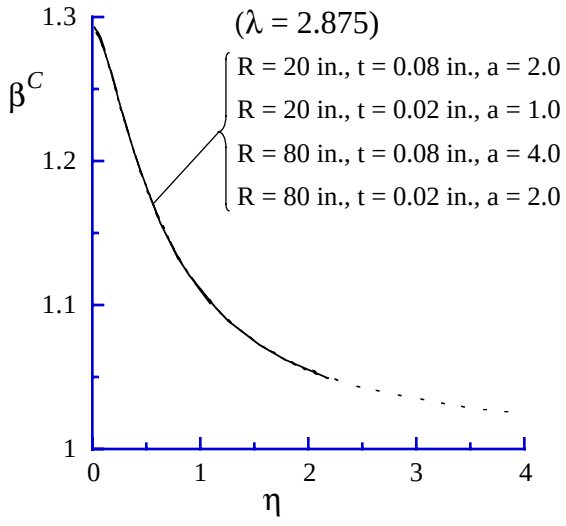

(b) β^C as a function of the nondimensional loading parameter.

Figure 6. Dependence of the bulging factor for a circumferential crack, β^C, on the loading parameter, η, for several values of the shell curvature parameter, λ.

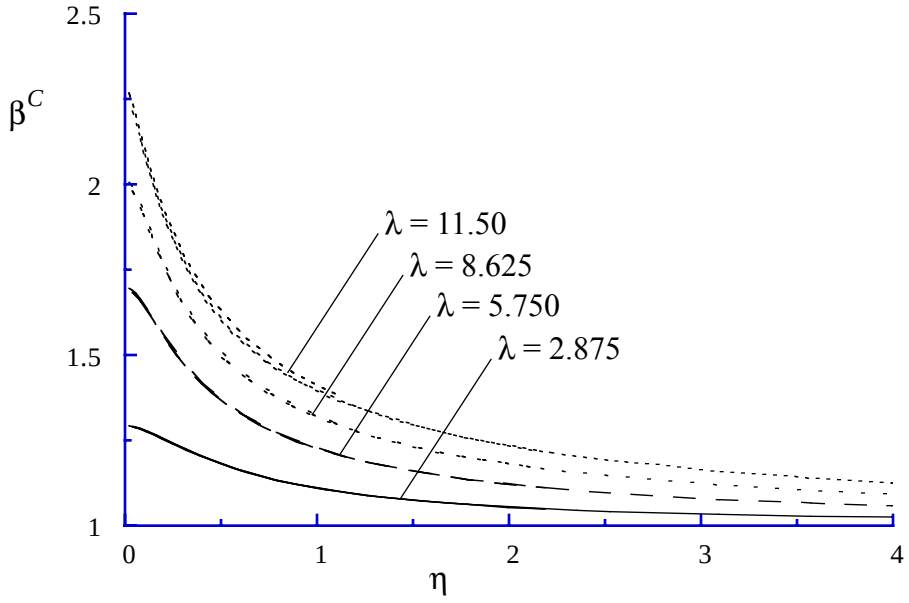

Figure 7. Contour plot of the bulging factor for a longitudinal crack, β^L, from STAGS analyses, as a function of the shell curvature parameter, λ, and the loading parameter, η.

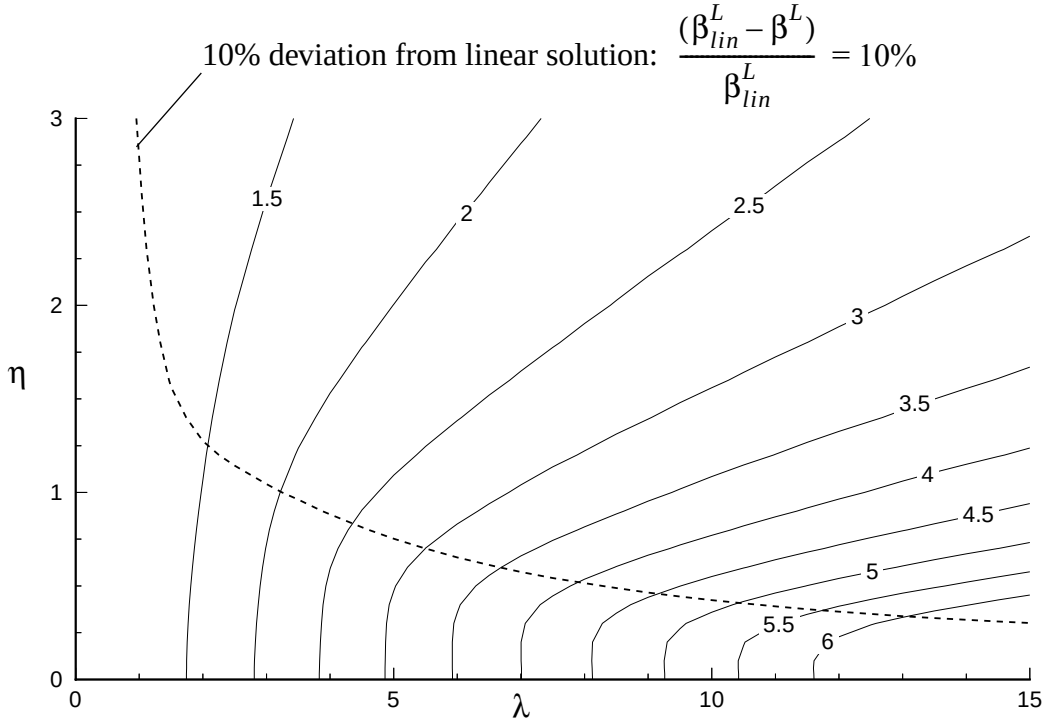

a common value of the bulging factor. The results in the contour plot indicate that the bulging factors monotonically increase with increasing values of λ, and monotonically decrease with increasing values of η. This behavior is consistent with the results shown previously in Fig. 4. In Fig. 7, for small values of η, the contour lines are perpendicular to the abscissa of the plot, indicating that when the loads are small, the bulging factor is a function of λ only. In this region of the plot, the behavior of the shell is dominated by the linear bending response, and the bulging factor for $\eta = 0$, i.e., for locations on the λ-axis, is exactly the linear response shown previously in Fig. 3a. For a given value of λ, at greater values of the loading parameter, the bulging factors decrease with increasing η, and the contour lines bend to the right and asymptotically approach lines which extend radially from the origin. The contour lines transition from being perpendicular to the horizontal axis to radial lines when the bending deformations become sufficiently large and cause nonlinear membrane stiffening. For higher values of load, the response is dominated by membrane tension effects which reduce the bulging factor. The dashed line in Fig. 7 indicates the location along which the bulging factor is 10% less than the linear bulging factor for the same value of λ. Thus, for values of (λ,η) that are below the dashed line, the bulging factor given by the linear solution is accurate to within 10%. For values of (λ,η) that are above the dashed line, a linear analysis would overpredict the bulging factor by more than 10%. The percentage difference between the bulging factor from the nonlinear analysis and the linear bulging factor for the same value of λ is shown for the entire range of λ and η in Fig. 8. The results shown here are consistent with the findings reported by Budiman and Lagace.[16]

Figure 8. Contour plot showing the percentage difference between the linear and nonlinear bulging factors for a longitudinal crack, as a function of the shell curvature parameter, λ, and the loading parameter, η.

$$\% \text{ difference} = \frac{(\beta_{lin}^{L} - \beta^{L})}{\beta^{L}}$$

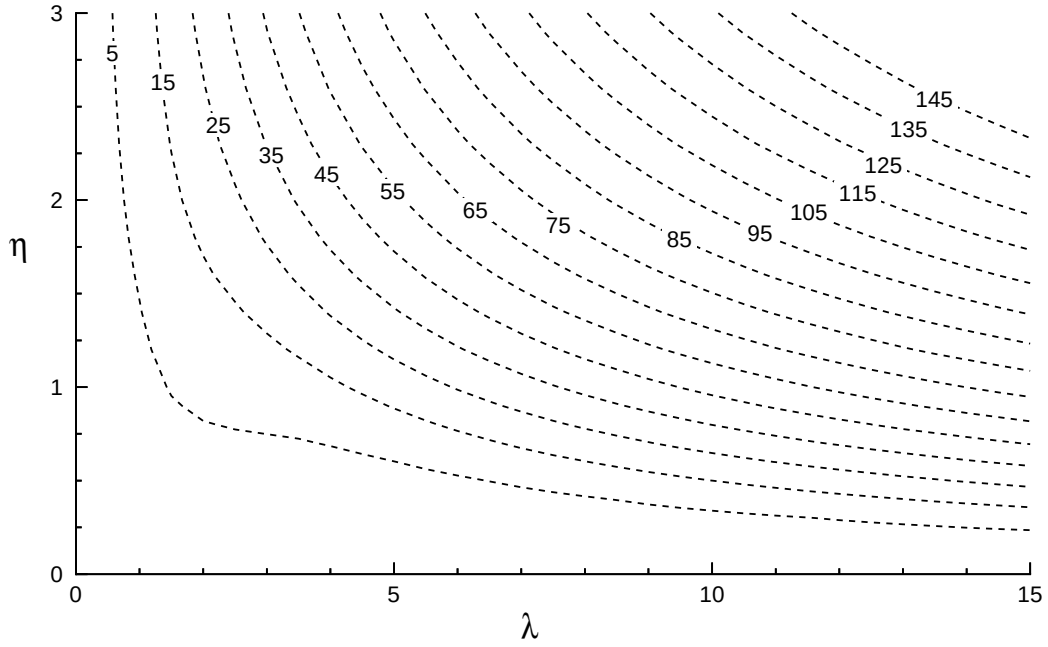

A simple expression for representing the bulging factor behavior shown in Fig. 7, that can be easily used in a design environment, is obtained by characterizing the linear and nonlinear regions of the response separately. The linear bulging factor for a longitudinal crack, β_{lin}^{L}, shown previously in Fig. 3a, is expressed as a function of λ by applying a polynomial curve fit to the numerical data.

Equation 8:

$$(\beta_{lin}^{L})^{2} = 0.937 + 0.189\lambda + 0.358\lambda^{2} - 0.133\lambda^{3} + 0.00030\lambda^{4}$$

The linear bulging factors from the STAGS analyses and the curve fit to the data are shown in Fig. 9a. An expression for estimating the nonlinear bulging factor is obtained by utilizing the fact that the contour lines asymptotically approach radial lines through the origin, and the value of the bulging factor can be uniquely related to the slope of the radial line, i.e., λ/η, to which a contour line asymptotically approaches. The nonlinear bulging factors from the top and right sides of Fig. 7 are plotted as function of λ/η in Fig. 9b, and then expressed as a function of λ/η by applying a polynomial curve fit to the numerical data.

Equation 9:

$$(\beta_{nl}^{L})^{2} = 0.768 + 1.323\left(\frac{\lambda}{\eta}\right) - 0.00286\left(\frac{\lambda}{\eta}\right)^{2}$$

Figure 9. Empirical curve fits of STAGS solutions for bulging factor for longitudinal cracks.

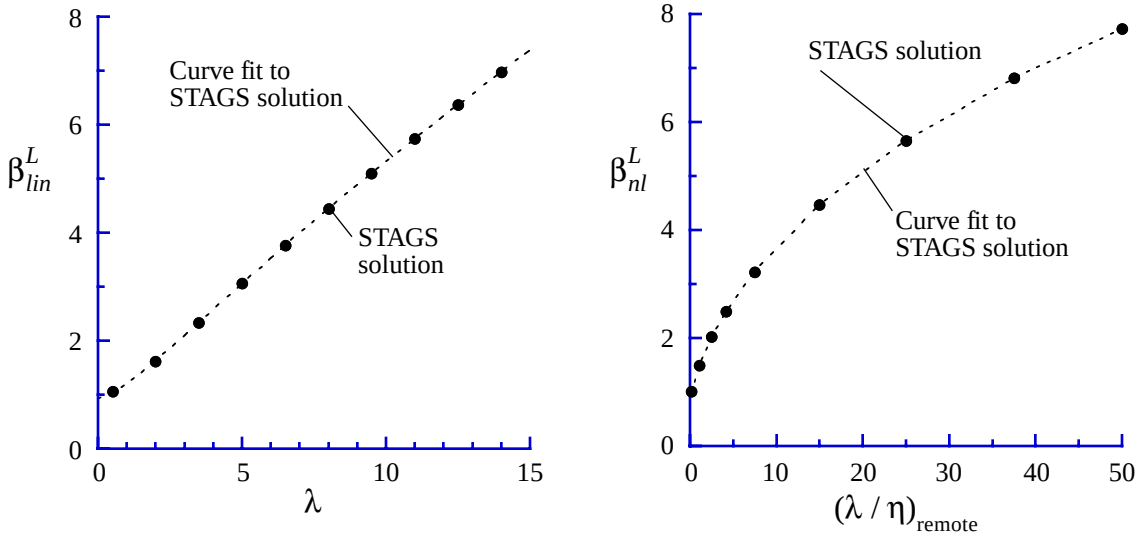

(a) Linear bulging factor for a longitudinal crack, β^L_{lin}, as a function of λ.

(b) Nonlinear bulging factor for a longitudinal crack, β^L_{nl}, as a function of remote values of the ratio λ / η.

The bulging factor for any value of λ and η, is estimated by taking the minimum of the linear bulging factor, estimated by Eq. (8), and the nonlinear bulging factor, estimated by Eq. (9).

Equation 10:

$$\beta^L = \min(\beta^L_{lin}, \beta^L_{nl}).$$

The bulging factors obtained by applying Eq. (10) are compared to the bulging factors from the STAGS analyses in Fig. 10. In Fig. 10, the bulging factors from the STAGS analyses are shown as solid lines, and the estimates from Eq. (10) are shown as dashed lines. The percentage difference between the bulging factor for a longitudinal crack computed using STAGS and approximated by Eq. (10) is shown as a function of λ and η in Fig. 11. As expected, the bulging factor results obtained using Eq. (10) generally agree well with the STAGS results, with a maximum difference of 12%. The largest errors in the estimation occur in the transition region from the linear bending response to the nonlinear membrane response. In this transition region, Eq. (10) overpredicts the bulging factor and thus provides a conservative estimate.

Circumferential Crack

The bulging factor results from STAGS analyses of cylindrical shells with circumferential cracks, β^C, are presented as a function of the shell curvature parameter, λ, and the loading parameter, η, in Fig. 12. The solid lines in the figure are contour lines, or lines through points with a common value of the bulging factor. The results in the contour plot indicate that the bulging factors

Figure 10. Contour plot showing the bulging factors for a longitudinal crack from the STAGS analyses, and from Eq. (10), as a function of the shell curvature parameter, λ, and the loading parameter, η.

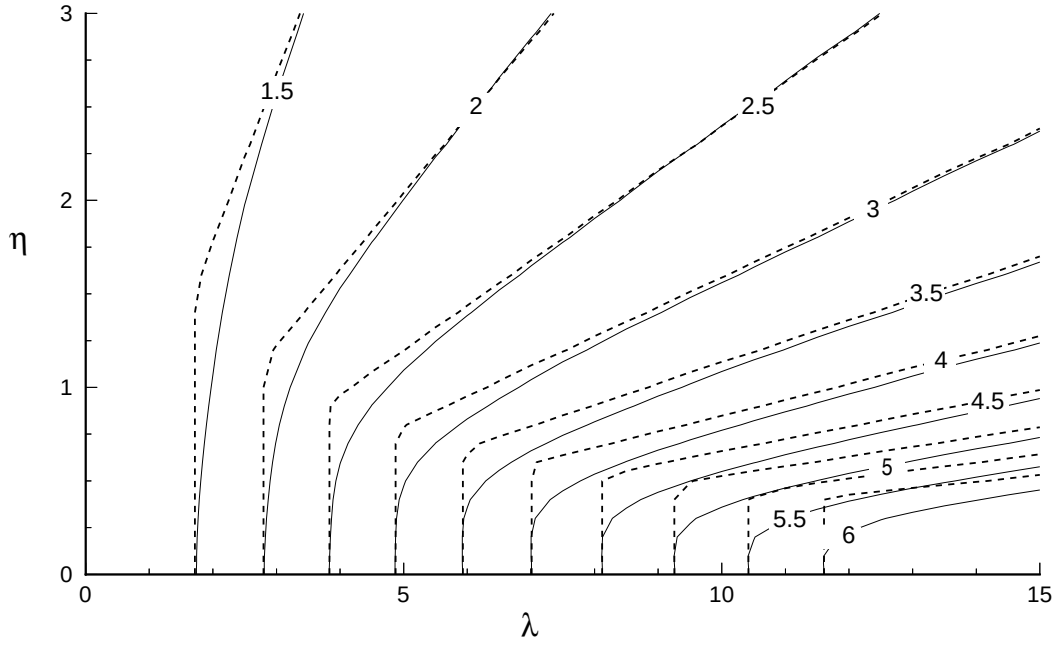

Figure 11. Contour plot showing the percentage difference between the bulging factors for a longitudinal crack as computed using STAGS and approximated by Eq. (10), as a function of the shell curvature parameter, λ, and the loading parameter, η.

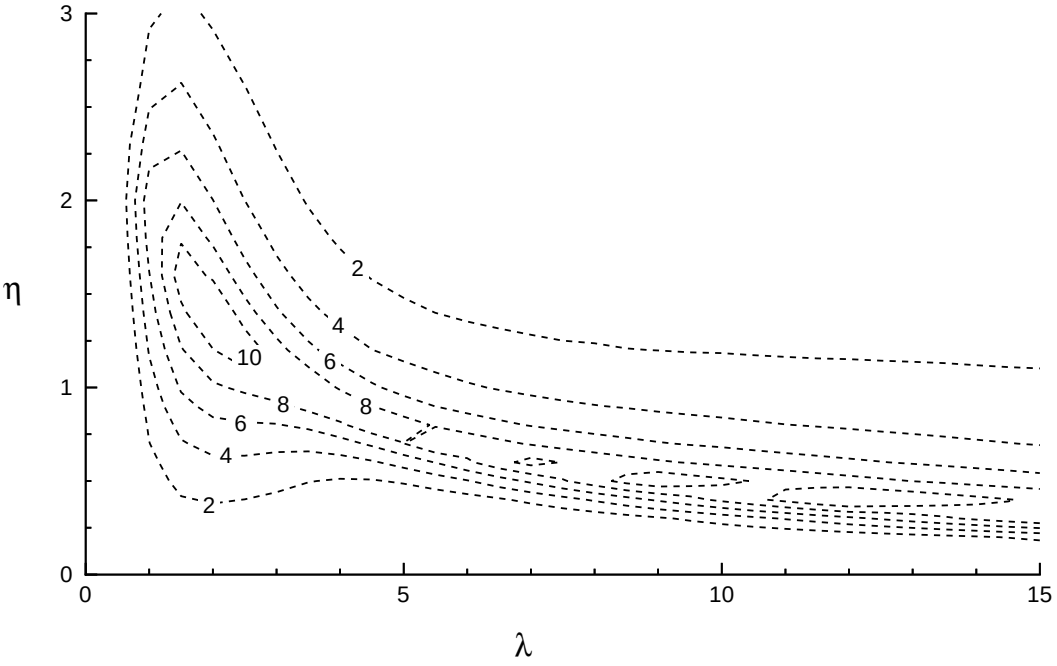

Figure 12. Contour plot of the bulging factor for a circumferential crack, β^C, from STAGS analyses, as a function of the shell curvature parameter, λ, and the loading parameter, η.

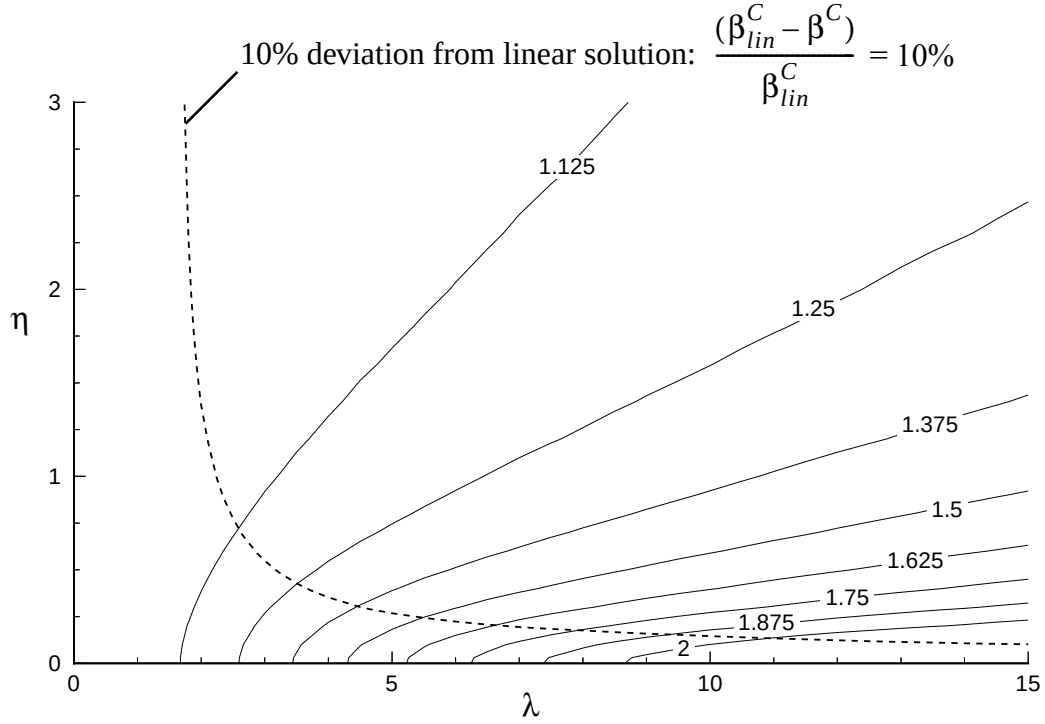

monotonically increase with increasing values of λ, and monotonically decrease with increasing values of η. This behavior is consistent with the results shown in Fig. 6. The contour plot of the bulging factors for the circumferential crack in Fig. 12 is similar to the contour plot of the bulging factors for the longitudinal crack shown previously in Fig. 7. The primary differences between the bulging factor contour plots for the two crack orientations are that the bulging factor for the circumferential crack is smaller in amplitude, and the contour lines are concentrated nearer to the abscissa of the plot. The bulging factor for $\eta = 0$, i.e., for locations on the λ-axis, is exactly the linear response shown previously in Fig. 3b. The contour lines are perpendicular to the λ-axis for very small loads, but the contours bend to the right almost immediately as η is increased, and asymptotically approach lines which extend radially from the origin. The dashed line in Fig. 12 indicates the location along which the nonlinear bulging factor is 10% less than the linear bulging factor for the same value of λ. This dashed line is closer to the λ-axis than it was for the longitudinal crack, indicating that the transition from the linear bending response to the nonlinear membrane response occurs at smaller values of load for a shell with a circumferential crack than for a shell with a longitudinal crack. The percentage difference between the bulging factor from the nonlinear analysis and the linear bulging factor for the same value of λ is shown for the entire range of λ and η in Fig. 13.

A simple expression, that can be easily used in a design environment, for representing the bulging factor behavior shown in Fig. 12 is obtained by characterizing the linear and nonlinear regions of the response separately. The linear bulging factor for a circumferential crack, β^C_{lin}, shown

Figure 13. Contour plot showing the percentage difference between the linear and nonlinear bulging factors for a circumferential crack, as a function of the shell curvature parameter, λ, and the loading parameter, η.

$$\% \text{ difference} = \frac{(\beta_{lin}^{C} - \beta^{C})}{\beta^{C}}$$

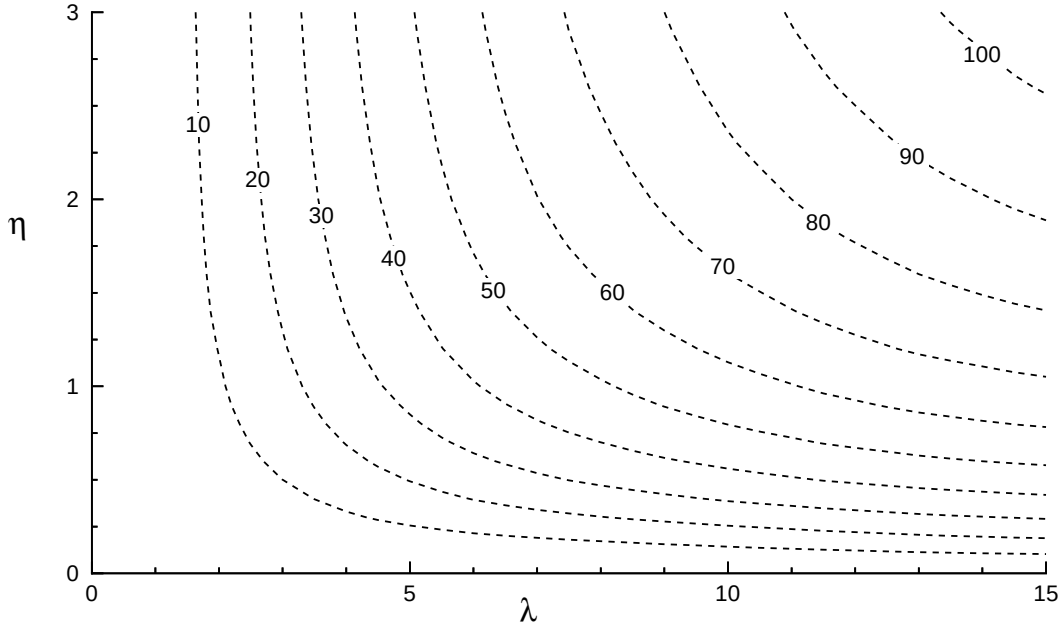

previously in Fig. 3b, is expressed as a function of λ by applying a polynomial curve fit to the numerical data.

Equation 11:

$$(\beta_{lin}^{C})^{2} = 0.955 + 0.110\lambda + 0.0637\lambda^{2} - 0.00534\lambda^{3} + 0.000144\lambda^{4}$$

The linear bulging factors from the STAGS analyses and the curve fit to the data are shown in Fig. 14a. An expression for estimating the nonlinear bulging factor is obtained by utilizing the fact that the contour lines asymptotically approach radial lines through the origin, and the value of the bulging factor can be uniquely related to the slope of the radial line, i.e., λ/η, to which the contour line asymptotically approaches. The nonlinear bulging factors from the top (η=3) and right (λ=15) sides of Fig. 12 are plotted as function of λ/η in Fig. 14b, and then expressed as a function of λ/η by applying a polynomial curve fit to the numerical data.

Equation 12:

$$(\beta_{nl}^{C})^{2} = 0.977 + 0.106\left(\frac{\lambda}{\eta}\right) - 0.00173\left(\frac{\lambda}{\eta}\right)^{2} + 1.43E\text{-}5\left(\frac{\lambda}{\eta}\right)^{3}$$

Figure 14. Empirical curve fits of STAGS solutions for bulging factor for circumferential cracks.

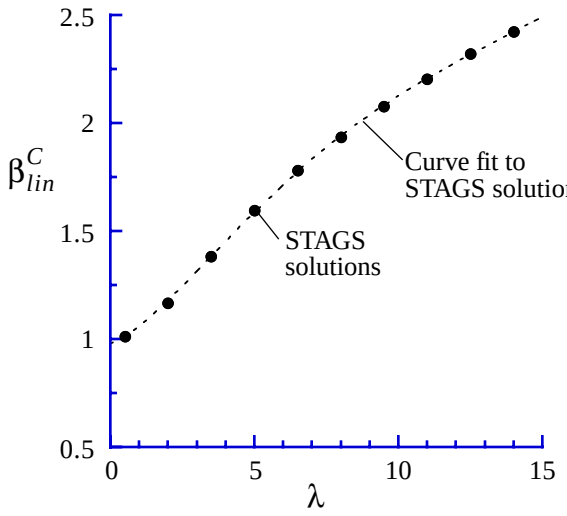

(a) Linear bulging factor for a circumferential crack, β^C_{lin}, as a function of λ.

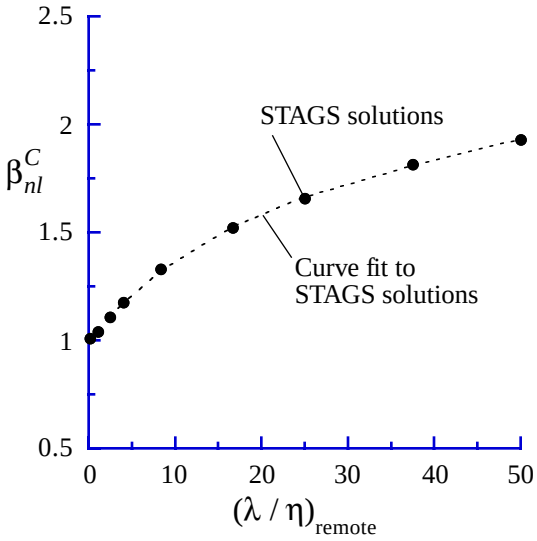

(b) Nonlinear bulging factor for a circumferential crack, β^C_{nl}, as a function of remote values of the ratio λ / η.

The bulging factor for any value of λ and η, is estimated by taking the minimum of the linear bulging factor, estimated by Eq. (11), and the nonlinear bulging factor, estimated by Eq. (12).

Equation 13:

$$\beta^C = \min(\beta^C_{lin}, \beta^C_{nl})$$

The bulging factors obtained by applying Eq. (13) are compared to the bulging factors from the STAGS analyses in Fig. 15. The bulging factors from the STAGS analyses are shown in Fig. 15 as solid lines, and the estimates from Eq. (13) are shown as dashed lines. The percentage difference between the bulging factors for a circumferential crack as computed using STAGS and approximated by Eq. (13) is shown as a function of λ and η in Fig. 16. As expected, the bulging factors as estimated by Eq. (13) generally agree well with the STAGS results, with a maximum difference of 12%. The largest errors in the estimation occur in the transition region from the linear bending response to the nonlinear membrane response. In this transition region, Eq. (13) overpredicts the bulging factor and thus provides a conservative estimate.

Comparison of Bulging Factor Results for Cylindrical Shells from Different Methods

Other methods in the literature for computing the bulging factor for a circumferential crack are based on the assumption of a geometrically linear response. The error incurred by applying a geometrically linear method to predict the geometrically nonlinear bulging factor for a circumferential crack was shown previously in Fig. 13.

Figure 15. Contour plot showing the bulging factors for a circumferential crack from the STAGS analysis, and from Eq. (13), as a function of the shell curvature parameter, λ, and the loading parameter, η.

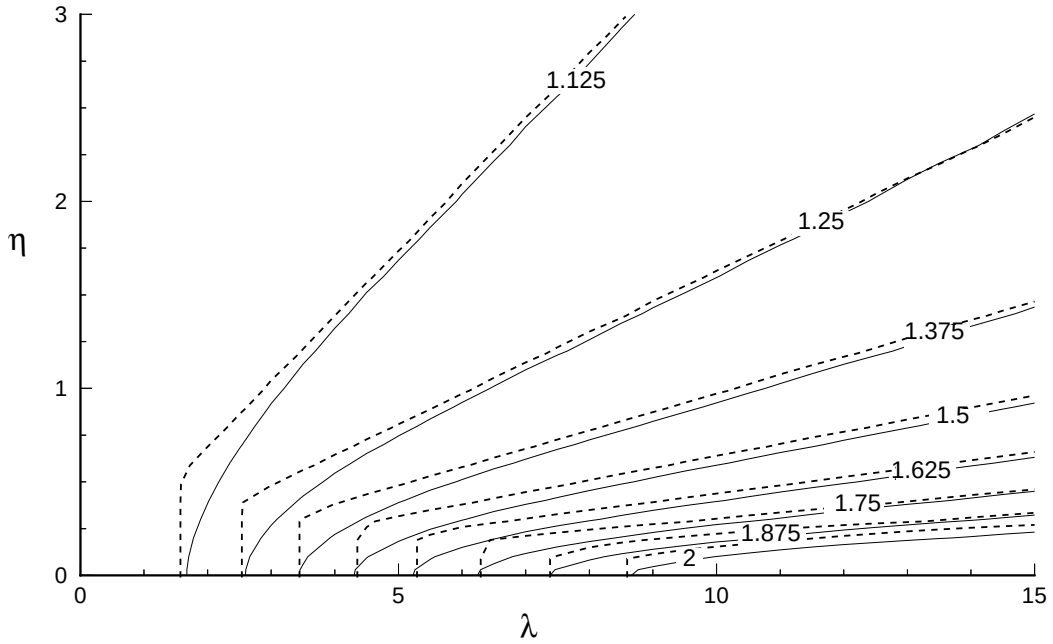

Figure 16. Contour plot showing the percentage difference between the bulging factors for a circumferential crack as computed using STAGS and approximated by Eq. (13), as a function of the shell curvature parameter, λ, and the loading parameter, η.

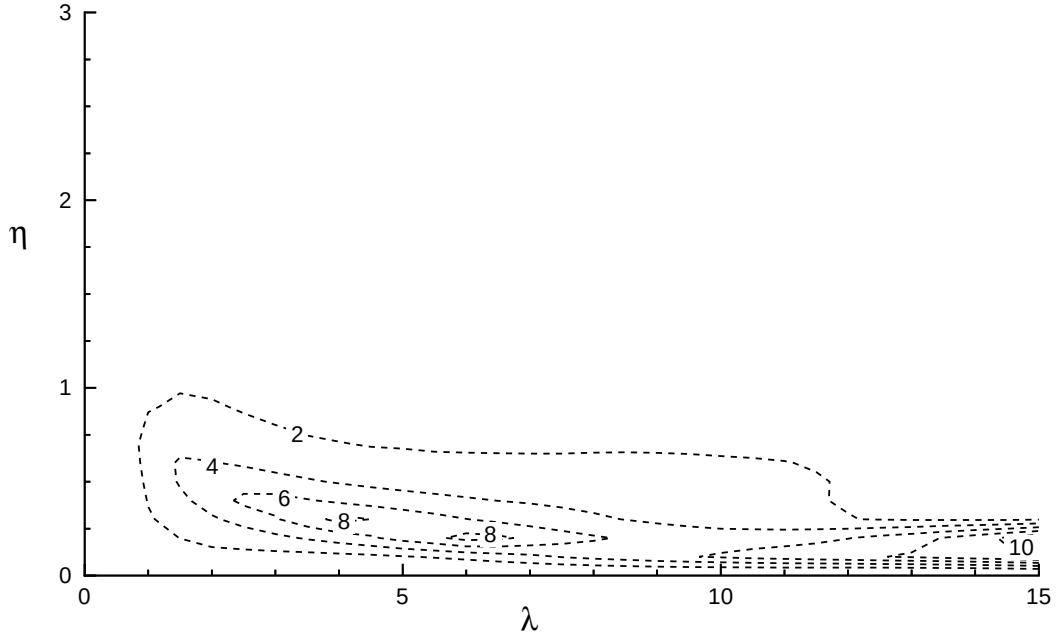

For the case of a cylindrical shell with a longitudinal crack, empirical expressions for predicting the bulging factor that approximately account for the geometrically nonlinear character of the bulging response have been developed. The most recent expressions were developed by Chen,[11] Jeong and Tong,[12] and Bakuckas et al.,[14] using a strain energy approach combined with dimensional analysis. The resulting relations for the bulging factor contain empirical constants that were determined from experimental data,[11,12] or from a geometrically nonlinear finite element parametric study.[13,14] The resulting relations developed by Chen,[11] Jeong and Tong[12] and Bakuckas et al.,[14] are provided in Eqs. (14), (15), and (16), respectively.

Equation 14:

$$\beta^L = \sqrt{1 + \frac{5}{3\pi}\frac{Eta}{R^2 p}\frac{0.316}{\sqrt{1+18\chi}}\tanh\left(0.06\frac{R}{t}\sqrt{\frac{pa}{Et}}\right)}$$

where $\chi = \sigma_x/\sigma_y$, and p is the internal pressure. The remote axial stress is σ_x and the remote hoop stress is σ_y. For the present paper, only the case with $\chi = 0.5$ is considered.

Equation 15:

$$\beta^L = \sqrt{1 + 0.671\left[\left(\frac{E}{\sigma_y}\right)\left(\frac{a}{R}\right)^2\right]^{2/3}}$$

Equation 16:

$$\beta^L = 1 + 0.775\left(\frac{E}{\sigma_y}\right)^{1/3}\left(\frac{a}{R}\right)^{5/6}$$

The empirical constants in Chen's expression, Eq. (14), were determined from fatigue crack growth tests of pressurized curved panels, with maximum remote hoop stress levels equal to 8.5 and 13.5 ksi. Tests were conducted for both uniaxial and biaxial loading conditions. In the tests, the biaxial load ratio $\chi = \sigma_x/\sigma_y$ was equal to zero for the uniaxial loading condition and equal to 0.24 for the biaxial loading condition. Chen tested seven shells, with geometries with $0.0025 \le a/R \le 0.05$ and $0.1 \le \lambda \le 2.0$. The empirical constant in Jeong and Tong's relation, Eq. (15), was determined from residual strength tests of curved panels with a radius $R = 75$ in. and with ratios of a/R between 0.06 and 0.10. Hoop stress levels were between approximately 5.0 and 12.5 ksi. The empirical constant in Eq. (16) was determined from a geometrically nonlinear finite element parametric study. The values of a/R ranged from 0.017 to 0.18, and the remote hoop stress level ranged from 5.0 to 20.0 ksi.

To evaluate the range of applicability of Eqs. (14 - 16), the percentage difference between the bulging factors from the nonlinear STAGS analyses and the bulging factors predicted by these equations are presented in Figs. 17-19. In these figures, contour plots show the percentage difference between the STAGS results and the results obtained using Eqs. (14 - 16) for the full range of the nondimensional parameters, $0 \le \lambda \le 15$ and $0 \le \eta \le 4$. Since Eqs. (14 - 16) are not expressed in terms of the nondimensional parameters λ and η, Eqs. (1) and (7) are used to compute the necessary parameters for given values of λ and η. These parameters are not unique for given values of λ and η, and are dependent on *(R/t)*. Therefore, the comparisons between the STAGS solutions

and the predictions from Eqs. (14 - 16) are presented for two configurations: (a) R = 20 in., t = 0.10 in.; and (b) R = 80 in., t = 0.04 in.

The percentage difference between the bulging factors from the nonlinear analysis and Eq. (14) is shown in Fig. 17. For the configuration with R = 20 in., the contour plot in Fig. 17a indicates that the predictions from Eq. (14) do not correlate well with the nonlinear analysis results, and the bulging factor predicted using Eq. (14) for this configuration may be up to 40% unconservative. For the configuration with R = 80 in., the contour plot in Fig. 17b indicates that the predictions from Eq. (14) correlate very well with the nonlinear analysis results for $\eta > 2$.

The percentage difference between the bulging factors from the nonlinear analysis and Eq. (15) is shown in Fig. 18. The results for both configurations are identical because the functional form in Eq. (15) is such that the dependence on *(R/t)* is eliminated. The results shown in Fig. 18 indicate that the bulging factors from Eq. (15) and the nonlinear analysis correlate well for $\eta > 1$. For large values of η, Eq. (15) predicts bulging factors that are up to 12% unconservative, and for $\eta < 1$ the predicted bulging factors become very conservative as η goes to zero.

The percentage difference between the bulging factors from the nonlinear analysis and Eq. (16) is shown in Fig. 19. The results indicate a small difference between the two configurations considered, but in general, the bulging factors from Eq. (15) and the nonlinear analysis correlate very well for $\eta > 1$. For $\eta < 1$, the predicted bulging factors become very conservative as η goes to zero.

The bulging factor expressions in Eqs. (14 - 16) are based on the assumption that the primary resistance to bulging deformation is due to membrane tension stress rather than due to bending stiffness, and thus, these expressions should correlate well with the nonlinear analysis results for configurations where the response is membrane dominated, but should not accurately represent a linear bending dominated response. The discrepancies, which can be quite substantial, between the results from Eq. (14) and the nonlinear analysis results are probably due to the limited range of parameters and experimental data that were used to obtain the empirical constants in Eq. (14).

Concluding Remarks

The results of a geometrically nonlinear parametric study to determine the effects of shell geometry and internal pressure loading magnitude on the stress intensity factors at the tips of longitudinal and circumferential cracks in thin unstiffened pressurized shells have been presented. The results are normalized by the stress intensity factor for flat plates, and presented in terms of the so-called crack "bulging factor" commonly used in design to represent the effects of shell curvature on the stress intensity factor. The results of the study are presented in terms of the shell curvature parameter, λ, which depends on the specific shell geometry, and the loading parameter, η, which depends on the magnitude of the applied internal pressure, the shell radius, and the material stiffness. The shell curvature parameter and loading parameter were suggested by Budiman and Lagace to be the nondimensional parameters for characterizing the nonlinear response of longitudinally and circumferentially cracked cylindrical shells.

The nonlinear finite element results of the present study agree with Budiman and Lagace's previous results for cylindrical shells with longitudinal cracks that showed that λ and η can be used to characterize the response of any cylindrical shell with a longitudinal crack. Furthermore, the results of the present study indicate that λ and η can also be used to characterize the geometrically

nonlinear response of any cylindrical shell with a circumferential crack. The results show that the magnitude of the bulging factor is affected by the shell geometry and the shell loading condition, and that for many shell geometries and load magnitudes the bulging factor is strongly influenced by the geometrically nonlinear response of a pressurized thin shell. The local response of the shell in the neighborhood of the crack is dominated by membrane or bending response characteristics depending on the values of the shell radius, the shell thickness, the crack length, and the magnitude of the applied internal pressure load. Simple empirical expressions for the bulging factor are derived from the numerical results and shown to predict accurately the nonlinear response of shells with longitudinal and circumferential cracks. The geometrically nonlinear results for the present study are compared with other results from the literature for the case of a longitudinally cracked cylindrical shell, and limitations on the use of these other results are suggested.

Figure 17. Contour plot showing the percentage difference between the bulging factors for a longitudinal crack, β^L, as computed using STAGS and approximated by Eq. (14), as a function of the shell curvature parameter, λ, and the loading parameter, η.

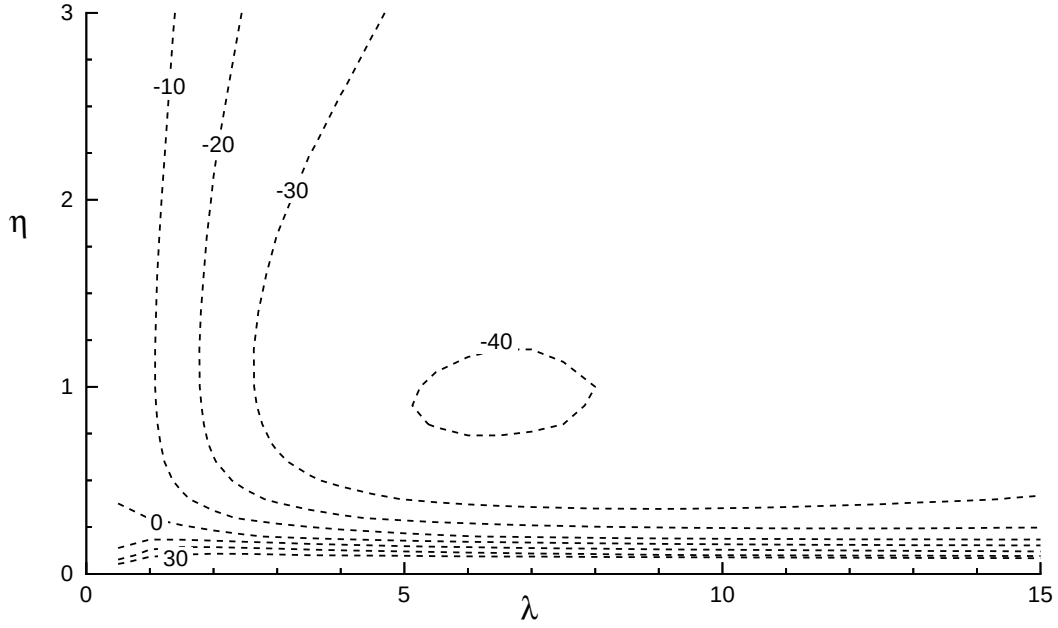

(a) R = 20 in., t = 0.10 in.

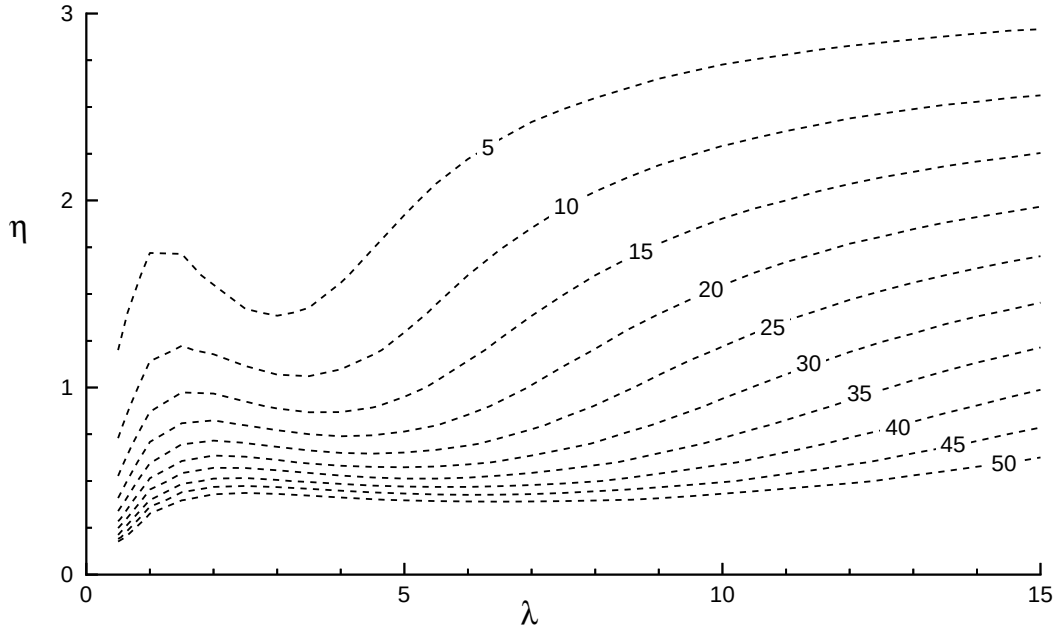

(b) R = 80 in., t = 0.04 in.

Figure 18. Contour plot showing the percentage difference between the bulging factors for a longitudinal crack, β^L, as computed using STAGS and approximated by Eq. (15), as a function of the shell curvature parameter, λ, and the loading parameter, η.

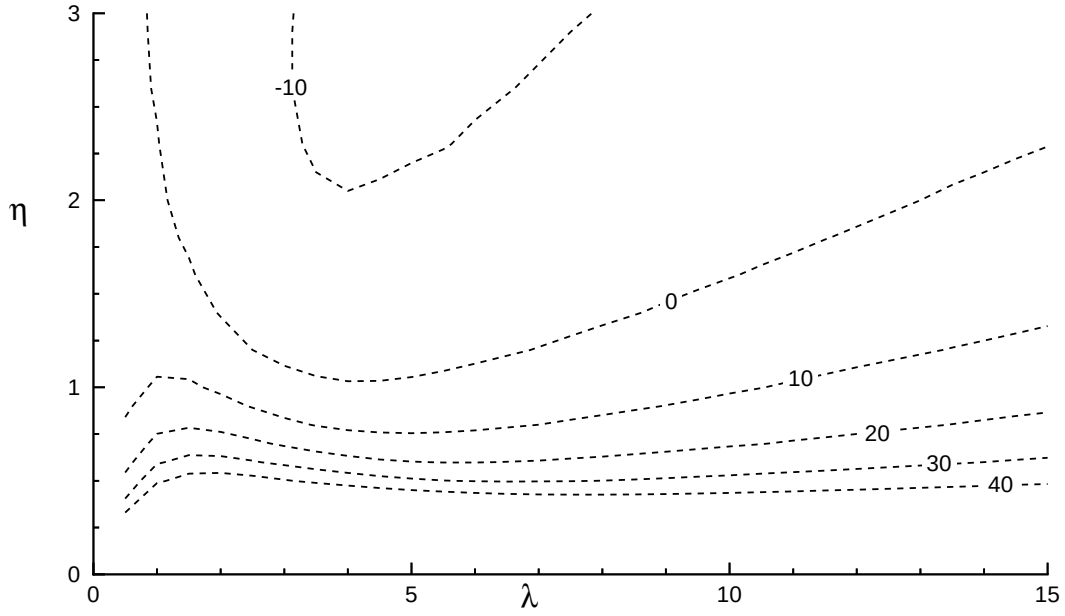

(a) R = 20 in., t = 0.10 in.

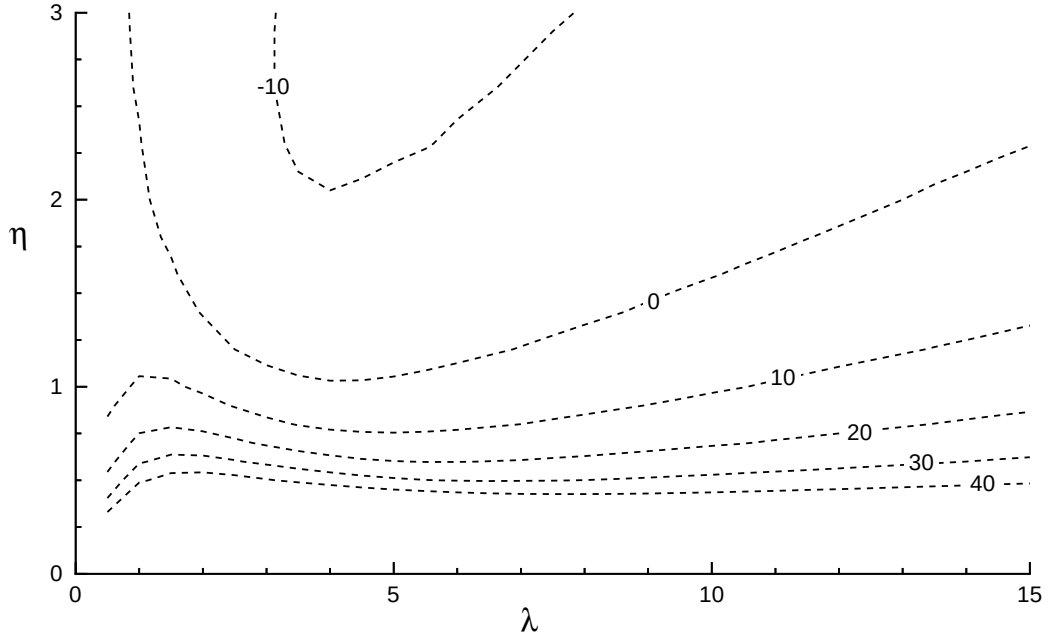

(b) R = 80 in., t = 0.04 in.

Figure 19. Contour plot showing the percentage difference between the bulging factors for a longitudinal crack, β^L, as computed using STAGS and approximated by Eq. (16), as a function of the shell curvature parameter, λ, and the loading parameter, η.

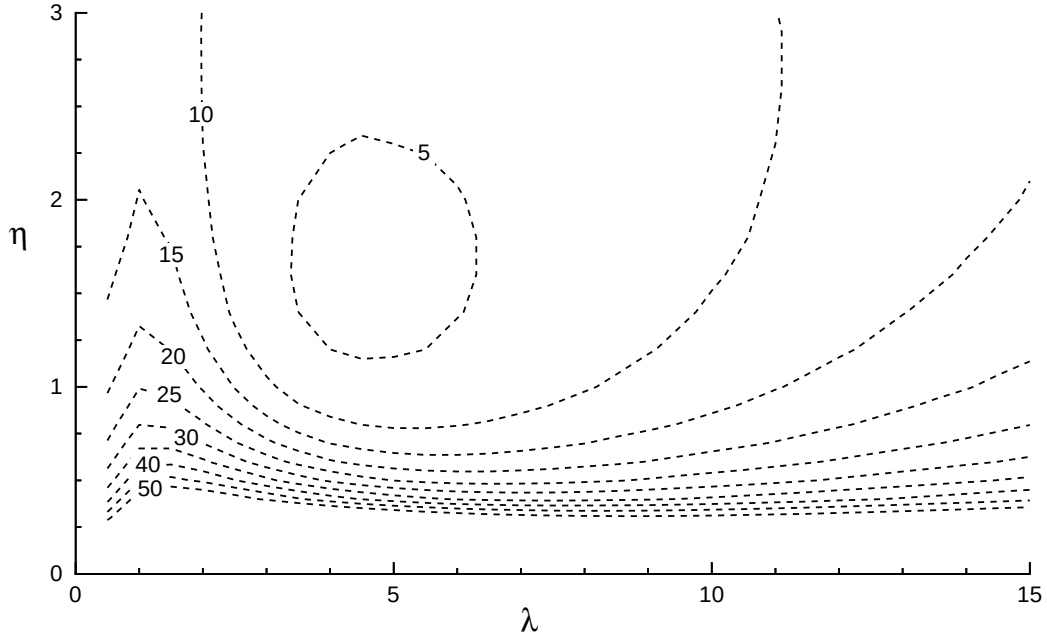

(a) R = 20 in., t = 0.10 in.

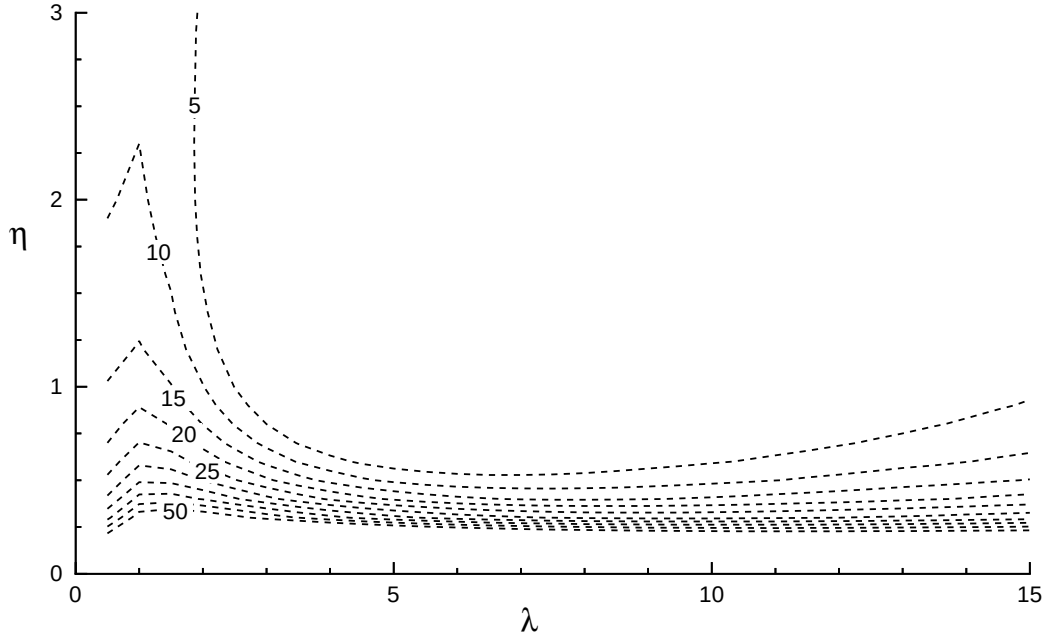

(b) R = 80 in., t = 0.04 in.

References

[1]Folias, E. S., "An Axial Crack in a Pressurized Cylindrical Shell," *International Journal of Fracture Mechanics*, Vol. 1, No. 2, 1965, pp. 104-113.

[2]Folias, E. S., "A Circumferential Crack in a Pressurized Cylindrical Shell," *International Journal of Fracture Mechanics*, Vol. 3, 1967, pp. 1-12.

[3]Folias, E. S., "On the Effect of Initial Curvature on Cracked Flat Sheets," *International Journal of Fracture Mechanics*, Vol. 5, No. 4, December, 1969, pp. 327-346.

[4]Folias, E. S., "Asymptotic Approximations to Crack Problems in Shells," *Mechanics of Fracture - Plates and Shells with Cracks*, G. C. Sih, H. C. van Elst, and D. Broek, eds., Noordhoff International, Leyden, pp. 117-160.

[5]Copely, L. G., and Sanders, J. L., Jr., "A Longitudinal Crack in a Cylindrical Shell under Internal Pressure," *International Journal of Fracture Mechanics*, Vol. 5, No. 2, June, 1969, pp. 117-131.

[6]Erdogan, F., and Kibler, J. J., "Cylindrical and Spherical Shells with Cracks," *International Journal of Fracture Mechanics*, Vol. 5, No. 3, September, 1969, pp. 229-237.

[7]Erdogan, F., and Ratwani, M., "Fatigue and Fracture of Cylindrical Shells Containing a Circumferential Crack," *International Journal of Fracture Mechanics*, Vol. 6, No. 4, September, 1970, pp. 379-392.

[8]Duncan-Fama, M. E., and Sanders, J. L., Jr., "A Circumferential Crack in a Cylindrical Shell under Tension," *International Journal of Fracture Mechanics*, Vol. 8, No. 1, March, 1972, pp. 15-20.

[9]Peters, Roger W., and Kuhn, Paul, "Bursting Strength of Unstiffened Pressure Cylinders with Slits," NACA TN 3993, April, 1957.

[10]Anderson, Robert B., and Sullivan, Timothy L., "Fracture Mechanics of Through-Cracked Cylindrical Pressure Vessels," NASA TN D-3252, February 1966.

[11]Chen, D., "Bulging of Fatigue Cracks in a Pressurized Aircraft Fuselage," Ph.D. Thesis, Delft University of Technology, Delft, The Netherlands, Report LR-647, October, 1990.

[12]Jeong, D. Y., and Tong, P., "Nonlinear Bulging Factor Based on R-Curve Data," Proceedings of the FAA/NASA International Symposium on Advanced Structural Integrity Methods for Airframe Durability and Damage Tolerance, September, 1994, pp. 327-338.

[13]Bakuckas, J. G., Ngugen, P. V., and Bigelow, C. A., "Engineering Fracture Parameters for Bulging Cracks in Pressurized Unstiffened Curved Panels," Proceedings of the FAA-NASA Symposium on Continued Airworthiness of Aircraft Structures, DOD/FAA/AR-97/2, 1996.

[14]Bakuckas, J. G., Jr., Nguyen, P. V., Bigelow, C. A., and Broek, D., "Bulging Factors for Predicting Residual Strength of Fuselage Panels," Presented at the International Conference on Aeronautical Fatigue, Edinburgh, Scotland, June 18-20, 1997.

[15]Riks, E., Brogan, F. A., and Rankin, C. C., "Bulging Cracks in Pressurized Fuselages: A Procedure for Computation," in Analytical and Computational Models of Shells, Noor, A. K., Belytschko, T., and Simo, J. C., Editors, The American Society of Mechanical Engineers, ASME-CED, Vol. 3, 1989.

[16]Budiman, H. T., Lagace, P. A., “Nondimensional Parameters for Geometric Nonlinear Effects in Pressurized Cylinders with Axial Cracks,” *Journal of Applied Mechanics*, Vol. 64, 1997, pp. 401-407.

[17]Budiman, H. T., “*Mechanisms of Damage Tolerance and Arrest in Pressurized Composite Cylinders*,” Ph.D. Thesis, Department of Aeronautics and Astronautics, Massachusetts Institute of Technology, Cambridge, MA, 1996.

[18]Yamaki, N., *Elastic Stability of Circular Cylindrical Shells*, (North-Holland Series in Applied mathematics and Mechanics), Vol. 27, E. Becker, B. Budiansky, W. T. Koiter, and H. A. Lauwerier, eds., North Holland, Amsterdam.

[19]Brogan, F. A., Rankin, C. C., and Cabiness, H. D., “STAGS User Manual,” Lockheed Palo Alto Research Laboratory, Report LMSC P032594, 1994.

[20]Broek, D., *Elementary Engineering Fracture Mechanics*, Sijthoff & Noordhoff, 1978.

[21]Riks, E., “Bulging Cracks in Pressurized Fuselages: A Numerical Study,” NLR Report NLR-MP-87058 U, NLR National Aerospace Laboratory, The Netherlands, 1978.

[22]Potyondy, D. O., Wawrzynek, P., A., and Ingraffea, A. R., “Discrete Crack Growth Analysis Methodology for Through Cracks in Pressurized Fuselage Structures,” *International Journal for Numerical Methods in Engineering*, Vol. 38, 1995, pp. 1611-1633.

[23]Riks, E., “Some Computational Aspects of the Stability Analysis of Nonlinear Structures,” *Computational Methods in Applied Mechanics and Engineering*, Vol. 47, 1984, pp. 219-259.

[24]Riks, E., “Progress in Collapse Analysis,” *Journal of Pressure Vessel Technology*, Vol. 109, Feb. 1987, pp. 27-41.

[25]Rybicki, E. F., and Kanninen, M. F., “A Finite Element Calculation of Stress Intensity Factors by a Modified Crack Closure Integral,” *Engineering Fracture Mechanics*, Vol. 9, 1977, pp. 931-938.

[26]Rose, C. A., Young, R. D., and Starnes, J. H., Jr., “Nonlinear Local Bending Response and Bulging Factors for Longitudinal Cracks in Pressurized Cylindrical Shells,” Presented at the 40th AIAA/ASME/ASCE/AHS/ASC Structures, Structural Dynamics, and Materials Conference, St. Louis, Missouri, April 12-15, 1999, AIAA Paper No. 99-1412.